Comparative first-principles analysis of electronic and absorption calculations of mono- and co-doped ZnO with trivalent ions Gd^{+3} and Al^{+3}

Ouahiba Ouadah, and Malika Dergal

Correspondence to: Ouahiba Ouadah (E-mail: *ouadah.ouahiba@gmail.com*)

ABSTRACT

In this paper, the energitics, electronic and absorption properties analysis doped with trivalent ions Gd^{+3} and Al^{+3} have been performed using first-principles calculations with the hybrid functional theory. The results show that the energetic stability can be easily prepared the desirables Gd-, Al-doped and Gd/Al-codoped ZnO at O-rich conditions. In addition, the incorporation of Gd^{+3} and Al^{+3} into ZnO lattice creates shallow donor states around Fermi level band minimum from mainly Al-3s and Gd-6s states, which offers good electronic properites with significant improvements for the Gd-doping compared to other dopants and pure ZnO. The results show that the absorption peaks of Al-doped and Gd/Al-codoped ZnO have a blue-shift compared with pure ZnO. However, the absorption of Gd/Al-codoped ZnO is slighly higher than that of pure and monodoped ZnO in the visible and infrared zone. Finally, these results confirm that trivalent ions doped-ZnO has n-type conductivity.

Introduction

Transparent conductive zinc oxides (ZnO) are devoted as promising II-VI group semiconductors materials in several areas for optoelectronic devices such as manufacturing transparent thin-film transistors, solar cells, and chemical sensors, etc [1-3]. Their advantages originate mainly from the wide and direct bandgap with high excitonic binding energy (60 meV) which allows significant excitonic emission at ambient temperature [4-7]. Unfortunately, ZnO is characterized by a low electrical conductivity, making its use in the optical field difficult. It has been argued that Rare-earth (RE) ions such as Tb, Er, and Gd are the better luminescent centers because of their intra-shell transitions which can generate narrow and intense emission lines [8, 9]. This is the reason why the rare-earth ions are considerably doped into oxide semiconductors for the modification of their electronic structure to accomplish new and enhanced electrical and catalytic properties while maintaining its good optical properties [10, 11]. Sa-Nguanprang et al. [12] demonstrated that Gd^{+3} ions acted as an effective electron scavenger to trap photo-induced electrons and inhibit electron-hole recombination. Obeid et al. [13] studied the structural and optical properties of the pristine and Gd-doped ZnO nanorods using a combination of experimental and theoretical approaches. The optical absorption spectrum of pure ZnO was improved at 6% Gd content. Structural characteristics of the synthesized Gd-doped ZnO nanoparticles investigated by X-ray diffraction and scanning thermoluminescence electron microscopy experiments revealed that the increase of Gd doping concentration resulted in a shift of thermoluminescence peaks at lower temperatures [14]. Another group has shown that the average transmission of Gd-doped ZnO thin films synthesized by the spray pyrolysis technique is greater than 75 % in the wavelengths ranging from 400 to 800 nm [15]. Besides, doping ZnO with Al^{+3} ions has received significant attention due to their remarkable lower cost and smaller atomic radius.

Dhamodharan et al. [16] revealed a higher transmittance around 95% for Al doped ZnO film in the visible region with an absorption edge around 350 nm, while the electrical resistivity decreased up to 1.5 at.% and increased for higher doping concentration. Tiron et al. [17] have been controlled ZnO: Al (AZO) thin films deposited by high-power impulse magnetron sputtering. Their results showed that AZO films are optically transparent with a limited electrical conductivity by the effect of decrease crystalline grain size. However, Shahid et al. [18] analyzed the formation of Al-doped ZnO thin films on glass by sol-gel process. They pointed out that 1 at.% Al doping ZnO film has the lowest resistivity (4.27 x 10^{-3} Ω cm) and higher charge carrier concentration (5.21 x 10^{19} cm^{-3}). El-Hamali et al. [19] have explored the electrical and optical characteristics of AZO films deposited by RF-magnetron sputtering at no intentional substrate heating. They found that the average visible transparency was enhanced from 85% to 90% and the bandgap was enlarged from 3.69 to 3.80 eV. Zhang et al. [20] concluded that the high doping Al concentration AZO nanoparticles prepared via the sol-gel combustion method present excellent photocatalytic activities and absorption capacities. Recently, increasing efforts have been given to the codoped ZnO with double ions to induce equilibrium electrical and optical properties in ZnO. Previously, very little experimental works have been reported the effect of rare-earth Gd concentration on the properties of AZO films. Anand et al. [21] were the first group who prepared Gd and Al co-doped ZnO thin films using nebulizer spray method with various Gd co-doping levels. Spray deposited pristine AZO films exhibited maximum optical transmittance 91% in entire wavelength spectrum while the minimum resistivity and maximum figure of merit values are detected for Gd co-doped AZO thin films. Hence, our main purpose of the present paper was to analyze the effect of Gd^{+3}, Al^{+3} doping ions on structural, electronic, and optical properties with a new insight into the influence of Gd^{+3}/Al^{+3} co-doped ZnO employing first principles simulation based on density functional theory (DFT).

Calculation Methods

In this paper, the first-principles calculations based on the density functional theory (DFT) was implemented in the Vienna Ab-initio Software Package (VASP) [22, 23]. Projector Augmented Wave (PAW) [24] pseudopotential is used to describe the interactions between electrons and ions. The valence electron configurations were $3d^{10}4s^2$ for Zn, $2s^22p^4$ for O, 6 s^2 $4f^75d^1$ for Gd and $3s^23p^1$ for Al. The exchange and correlation energy have been performed using the Generalized Gradient Approximation (GGA) within Perdew, Burke, and Ernzerhof (PBE) scheme [25], and Hybrid Susceria-Enzeroft (HSE) [26, 27]; where HSE provides much better band gaps results and the most accurate electronic structure. It is well known that the wurtzite structure of ZnO is considered the most energetically stable. The wurtzite unit cell formed by four atoms where Zn occupied the sites (1/3, 2/3, 0) and (1/3, 2/3, 1/2), while O atoms alternatively occupy the positions (2/3, 1/3, *u*) and (2/3, 1/3, 1/2+*u*) ; as shown in Figure 1 (a). Where *u* is an internal parameter. To describe the pure semiconductor, we have used a plane-wave basis set with a 500 eV energy cutoff, and the Brillouin Zone (BZ) was sampled using different Monkhorst–Pack (MP) [28] grids including the Γ point in the calculations; 10×10×8 k-point mesh for pure ZnO by the GGA-PBE approximation, and 6×6×4 k-point mesh for the HSE approach. Furthermore, we used k-point meshes of 6×6×4 GGA-PBE and 2×2×2 HSE for a (2×2×4) supercell model consisting of 64 atoms, as shown in Figure 1 (b). The Brillouin zone integration was performed via the tetrahedron [29] method with a 0.05 eV smearing of the electron levels. Full atomic relaxations were executed by minimizing the ionic Hellman-Feynman force [30] until the maximum forces achieved less than 0.02 eV/Å.

(a)

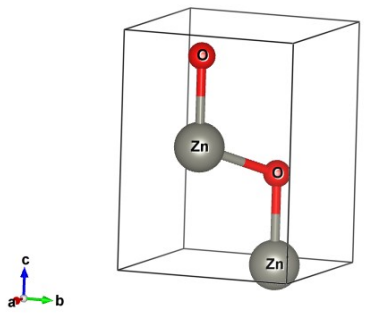

(b)

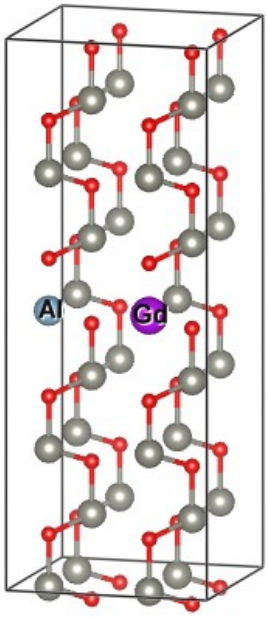

Figure 1. (a) Unit cell of ZnO, (b) 2 x 2 x 4 supercell of Gd/Al-codoped ZnO model.

Results and discussion

Geometrical optimization and formation energy

The lattice constants and average bond lengths after the structural optimization are presented in table 1. The optimized crystal parameters of pure ZnO are consistent with experimental and theoritical values. On the other hand, the relaxed ZnAlO, ZnGdO and Al/Gd-codoped systems depict an obvious change in the lattice parameters compared to the pure ones. From table 1, we can also see that the Zn–O bonds were slightly longer than those in the pure ZnO. This is may be attributed to the difference of atomic radius between Al (1.18Å), Gd (2.33Å) and Zn (1.42 Å). As a result, the substitutional atoms caused an internal distortion along the [100] and [001] directions. The bond length order was *O-Al* < *Zn-O* < *Zn-Al* < *O-Gd*. X-ray diffraction and XPS results revealed that the doping of Gd ions has a minor effect on the internal structure of ZnO [35].

In order to explore the stability of Gd-, Al- and Gd/Al-doping systems, the formation energies of the pure, doping and codoping ZnO were computed according to the following formulas:

$$\Delta E_{form}^{ZnO} = E_{tot}^{ZnO} - (\mu_{Zn} + \mu_O) \quad (1)$$

$$\Delta E_{form} = E_{doped(Al)} - E_{pure} + \mu_{Zn} - \mu_{Al} \quad (2)$$

$$\Delta E_{form} = E_{doped(Gd)} - E_{pure} + \mu_{Zn} - \mu_{Gd} \quad (3)$$

$$\Delta E_{form} = E_{codoped} - E_{pure} + n_{Zn}\mu_{Zn} - \mu_{Al} - \mu_{Gd} \quad (4)$$

Where : $E_{codoped}$, E_{doped} and E_{tot}^{ZnO} are the total energy with and without dopant, n_{Zn} indicate the number of Zn atoms removed; n_{Gd} and n_{Al} are the number of Gd and Al atoms that have been incorporated to the ZnO supercell; μ_{Zn}, μ_O, μ_{Gd} and μ_{Al} are the chemical potentials of Zn, O, Gd and Al elements, respectively.

To investigate the environment effect on chemical potentials, we consider the following two different conditions:

Table 1. Lattice parameters, the average bond lengths and the formation energy of ZnO systems with and without doped and co-doped elements.

Compounds	a_{eq}(Å)	c_{eq}(Å)	Bond lengths					ΔE_{form} (eV/atom)	
			Zn-O	*Zn-Al*	*Zn-Gd*	*O-Al*	*O-Gd*		
ZnO	3.280^{GGA}	5.290^{GGA}	1.995^{GGA}	--	--	--	--	-3.50^{GGA}	
	3.255^{HSE}	5.251^{HSE}	1.977^{HSE}	--	--	--	--	-4.19^{HSE}	
	3.249[a]	5.206[a]						-3.60[d]	
	3.285[b]	5.292[b]							
	3.253[d]	5.254[c]							
								Zn-rich	*O-rich*
$Zn_{0.96875}Al_{0.03125}O$	3.296^{GGA}	5.305^{GGA}	1.997^{GGA}	3.311^{GGA}	3.317^{GGA}	1.832^{GGA}	2.155^{GGA}	-5.09^{GGA}	-8.63^{GGA}
	3.262^{HSE}	5.253^{HSE}	1.978^{HSE}	3.304^{HSE}	3.308^{HSE}	1.795^{HSE}	2.157^{HSE}	-5.82^{HSE}	-9.47^{HSE}
$Zn_{0.96875}Gd_{0.03125}O$	3.311^{GGA}	5.327^{GGA}	2.000^{GGA}	3.315^{GGA}	3.319^{GGA}	1.834^{GGA}	2.157^{GGA}	-3.04^{GGA}	-6.53^{GGA}
	3.276^{HSE}	5.277^{HSE}	1.981^{HSE}	3.308^{HSE}	3.310^{HSE}	1.798^{HSE}	2.158^{HSE}	-4.12^{HSE}	-7.31^{HSE}
$Zn_{0.9375}Al_{0.03125}Gd_{0.03125}O$	3.310^{GGA}	5.329^{GGA}	1.998^{GGA}	3.314^{GGA}	3.318^{GGA}	1.834^{GGA}	2.157^{GGA}	-4.56^{GGA}	-11.53^{GGA}
	3.275^{HSE}	5.264^{HSE}	1.979^{HSE}	3.307^{HSE}	3.310^{HSE}	1.797^{HSE}	2.158^{HSE}	-5.02^{HSE}	-12.14^{HSE}

i) Under O-rich conditions, where μ_O is calculated from the ground-state energy of the O_2 molecule ($\mu_O = \mu_{O_2}/2$), while μ_{Zn} is obtained by growth condition ($\mu_{Zn} = \mu_{ZnO} - \mu_O$).

ii) Under Zn-rich conditions, where μ_{Zn} is assumed to be the energy of bulk metal Zn ($\mu_{Zn} = \mu_{Zn(metal)}$), and μ_O is determined by ($\mu_O = \mu_{ZnO} - \mu_{Zn}$).

The formation energy results of pure, doped and codoped ZnO systems using both GGA-PBE and HSE approximations are listed in table 1. The calculated formation energy of pure ZnO by

GGA-PBE is in agreement with the available experimental finding, while the HSE approximation slightly overestimates this value. It can be seen that the formation energies are negative for all studied systems, which means that they are thermodynamically stable. The obtained results show that the Gd and Al impurities prefer to substitute Zn atoms under O-rich and Zn-rich conditions. We further report that the Gd-, Al- and Gd/Al-doping systems can be easily prepared under O-rich conditions since their ΔE_{form} values are much lower than of the Zn-rich conditions.

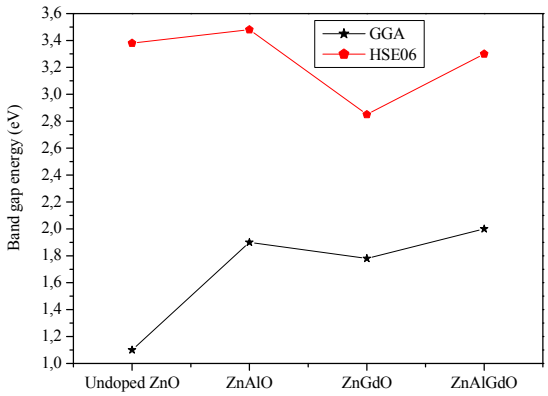

Figure 2: Variation of band gap energy as a function of the dopant.

Electronic property analysis

Band gap variation

Wide-band gap semiconductors are semiconductor materials which have a relatively large band gap compared to conventional semiconductor [36]. Generally, the band gap determines how much energy is required from the sun for conduction, as well as how much energy is generated. Figure 2 reveals the variation of band gap energy for ZnO without and with dopant. The band gap energy of pure ZnO calculated by GGA-PBE is about 1.10 eV, which is largely underestimated compared to the experimental value obtained by Mang et al. [37] (3.44 eV). To overcome this situation, it has been reported that the HSE technique yields energy gaps of semiconductors in better agreement with experiment than the widely utilitized semilocal PBE functional [38, 39]. The calculated band gap value of pure ZnO using HSE is 3.39 eV, which is consistent with the experimental one.

The optical band gap of Gd^{+3}-, Al^{+3}-monodoped and Gd^{+3}/Al^{+3}-codoped ZnO models was larger than the band gap of pure ZnO model. By comparing the optical band gap values of these systems, the most lowest band gap energy is found for Gd-doped ZnO model (1.79 eV by GGA-PBE, and 2.86 eV by HSE). Deepa Rani et al. [40] have suggested also that the band gap value is decreased when increasing the concentration of Gd. On the other side, a significant improvement has been detected for Al-doped ZnO model (1.93 eV by GGA-PBE, and 3.50 eV by HSE). The optical studies of Al doped ZnO films exhibited a maximum value of energy gaps in the range 3.73-3.83 eV [41]. The optical band gap analyzed by Lin et al. [42] at room temperature was found to be 3.38 eV for pure ZnO film and 3.58 eV for ZnO: Al (AZO) films while it drops to 3.45 eV for AZO films doped with Gd.

Compared to the mono-doped systems, the optical band gap value of Gd^{+3}/Al^{+3}-codoped ZnO model was between those of Al-, Gd-doped ZnO models. Wang et al. [43] investigated the structural and optical properties of low temperature hydrothermal synthesized (Gd, Al)-codoped ZnO nanoparticules. They found that band gap of $Zn_{0.96-x}Gd_xAl_{0.04}O$ increases from 3.46 to 3.62 eV with increasing Gd-doping concentration. The increase of energy bandgap is a result of occupying of the lowest orbitals in

the CB by electron introduced by Gd or Al doping—Moss–Burstein effect [47].

Density of states

To study the effect of the incorporation of Gd^{+3}, Al^{+3} and Gd^{+3}/Al^{+3} into the ZnO lattice on the electronic properties, we have compared the calculated density of states of these systems. The total and partial densities of states (Total and PDOS) of pure, doped and codoped ZnO are computed using GGA-PBE and HSE06 approximations and presented in Figure (3-4-5-6). The Fermi level is taken as the reference level which is set at zero.

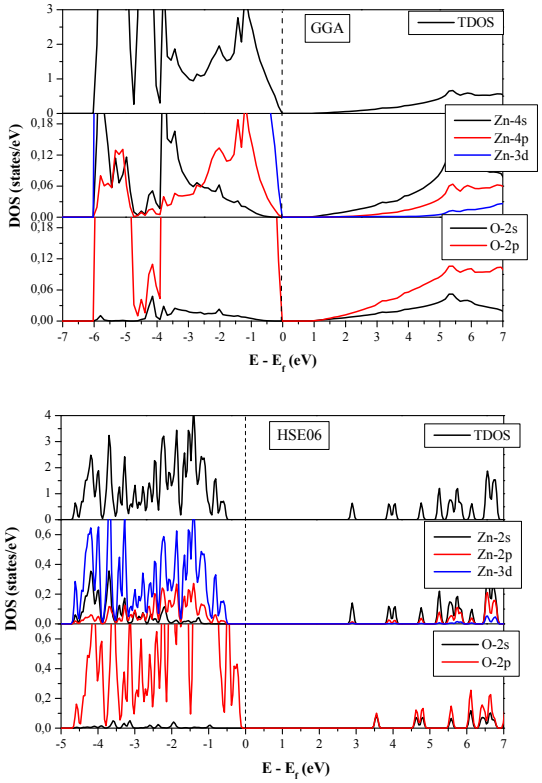

Figure 3 : Density of states of pure ZnO using : (a) GGA, (b) HSE06.

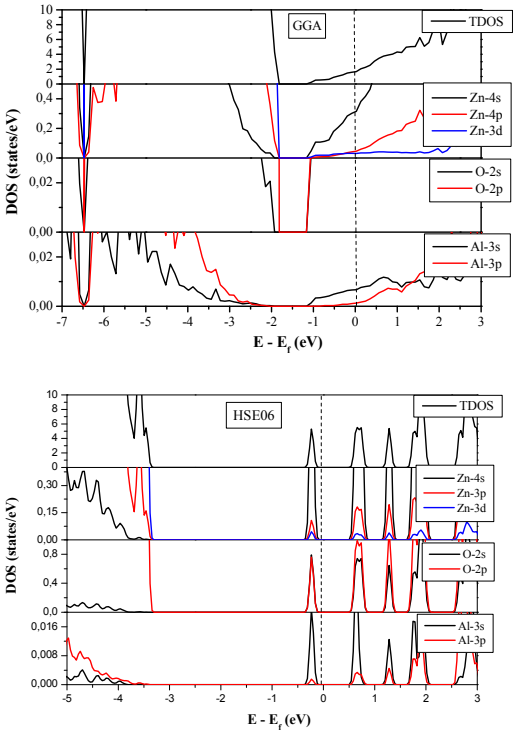

Figure 4 : Density of states of Al-doped ZnO using : (a) GGA, (b) HSE06.

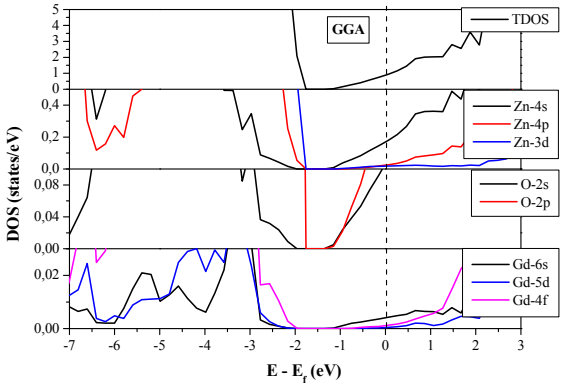

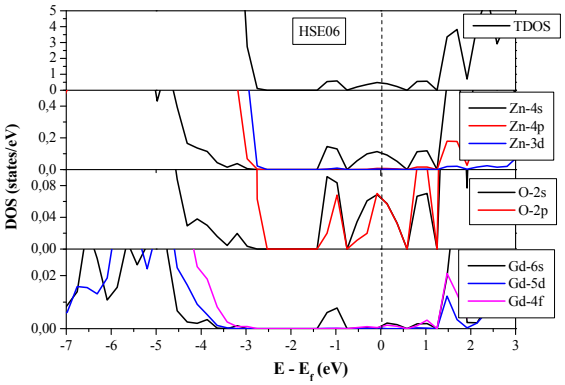

Figure 5 : Density of states of Gd-doped ZnO using : (a) GGA, (b) HSE06.

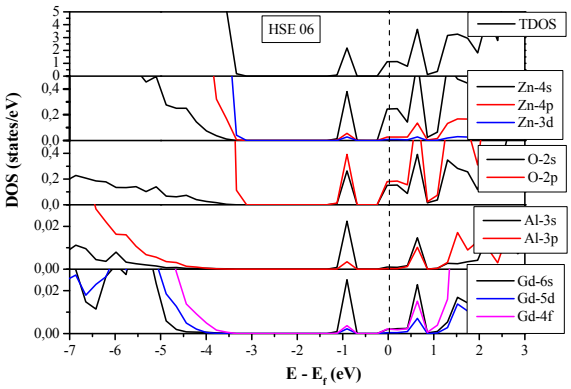

Figure 6 : Density of states of Gd/Al-codoped ZnO using : (a) GGA, (b) HSE06.

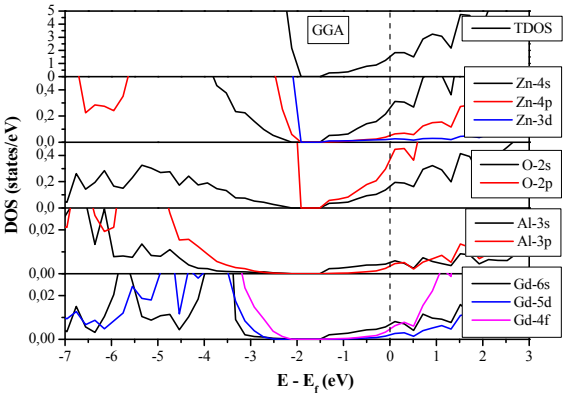

From Figure 3, we can see that the total state density has two regions in the valence band: a deep region less than -4 eV dominated by O-2p states, the second one (-4 eV ~ -1 eV) is constituted by O-2p and Zn-4p states, which are separated by a strong hybridization where Zn-4p states forming a peak at about -1 eV which is more localized contributes to the strong covalence in Ti-d_¿Al-p bonds. The conduction band dominated mainly by Zn-4s states.

By comparing the state densities of doping and codoping ZnO models, the most interesting feature that can be seen in Figure (4-5-6) is the Fermi level shift towards the bonding area of the conduction band by adding a concentration *x=3.125 %* of Gd^{+3}, Al^{+3} and Gd^{+3}/Al^{+3} into the ZnO supercell. The conduction band mainly consists of s, p and f orbitals of Zn, O, Al, and Ga atoms, and the donor states are contributed by the s and p orbitals of the constituent Zn and O atoms and the Al−*3s* and Gd−*6s* states. To evaluate the contribution of each dopant to the carrier concentration, the shallow donor states for all atoms and each dopant were integrated. It can be seen that Gd atoms contribute more free carriers than Al atoms. Hence, we can predict that Gd atoms contribute more free carriers than Al atoms in the monodoped and codoped models, which benefit conductive ability. In other words, more free carriers participate in the electrical transport process when Gd is incorporated in ZnO.

Absorption property analysis

The optical properties can be described by the complex dielectric response function, ε(ω), which is defined as $\varepsilon(\omega) = \varepsilon_1(\omega) + i\varepsilon_2(\omega)$ in linear response range. The real part $\varepsilon_1(\omega)$ of the dielectric constant is computed by the usual Kramers-Kronig relations [44].

$$\varepsilon_1(\omega)=1+\frac{2}{\pi}P\int_0^{\infty}\frac{\omega' \varepsilon_2(\omega')}{\omega'^2-\omega^2-i} \quad (5)$$

The imaginary part $\varepsilon_2(\omega)$ of the dielectric constant is given from the momentum matrix elements taken away the occupied and unoccupied states using the equation:

$$\varepsilon_2(\omega)=\frac{4\pi^2 e^2}{\Omega}\lim_{q}\frac{1}{q^2}\sum_{c,v,k} 2w_k \delta(\varepsilon_{ck+e_{1q}}-\varepsilon_{vk}-\omega)\left\langle u_{ck+e_{1q}}\middle|u_{vk}\right\rangle\left\langle u_{ck+e_{2q}}\middle|u_{vk}\right\rangle^{*} \quad (6)$$

Where *c* and *v* are the indices defining the conduction and valence band states, respectively. ε_{ck} and ε_{vk} are the energy levels. $u_{ck+e_{1q}}$ and $u_{ck+e_{2q}}$ are defined as the cell periodic part of orbitals at the k-point. Ω and *e* represent the volume of the primitive cell and the elementary charge, respectively. e_1 and e_2 are components of the unit vector.

In general, the absorption of radiation by matter is the process in which the energy of a photon is absorbed by matter, via electrons or atoms. The pure ZnO is known for its low absorption in the visible and near IR region of light. The absorption coefficient α(ω) of the material can be computed directly from the dielectric function by the following formula:

$$\alpha(\omega)=\sqrt{2}\left(\frac{\omega}{c}\right)\left[\sqrt{\varepsilon_1^2(\omega)-\varepsilon_2^2(\omega)}-\varepsilon_1^2(\omega)\right] \quad (7)$$

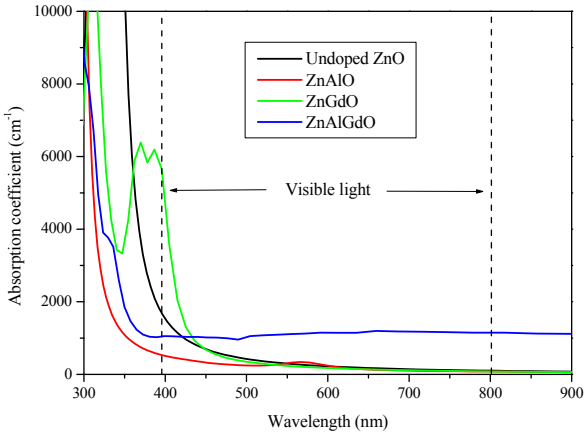

Figure 7: The calculated absorption coefficients of Gd-, Al-doped and Gd\Al-codoped ZnO compared with the undoped system using HSE06 approximation.

Figure 7 displays the absorption curve versus photon wavelenght of pure, doped and codoped ZnO models. Indeed, the results of pure ZnO reveal a slight absorption in infrared and visible range of light. The Al-doped and Gd/Al-codoped ZnO models allow the extension of the absorption edge towards lower wave lengths. Comparing these systems, the absorption edge decreased from about 340 nm in the case of Al-doped ZnO to 355 nm in the case of Gd/Al codoped ZnO. The shift in the absorption edge may be attributed to the increase of the band gap energy as a function of the dopant. Moreover, the blue shifted of UV absorption edge is due to the occupied states close to conductional band minimum; which are shallow donor states and the broadening of the optical band gap. On the other hand, Gd-doped ZnO model shifts the absorption edge towards higher wave lengths. It appears also that Gd/Al codoped ZnO increases slighly the absorption coefficient compared to the pure and doped systems. The obtained finding indicates that Al doping ZnO shows good optical characteristics in the visible and infrared region and exhibited

a sharp absorption edge at a wavelenght below 400 nm. UV-VIS spectra analyzed by Sahu et al. [45] showed red-shift of absorption band of ZnO with Gd doping element. The optical analysis of ZnO: Al films made by Osanyinlusi et al. [46] showed a maximum value of transmittance ranging from 82% to 91% depending on the condition of the films.

Conclusions

To sum up, we performed hybrid first-principle calculations to examine the Gd-, Al-doped and Gd\Al-codoped effect on the structural, electronic and optical properties of ZnO. The calculated results show that HSE06 hybrid functional appropriately corrects the shortcomings of standard PBE approximation for electronic structure. The analysis showed that the lattice parameters of Al and Gd doped ZnO change little comparing with pure ZnO. The calculated energetic results indicate that the Gd\Al-codoped ZnO can be easily prepared at O-rich conditions. The electronic structures show that the Fermi level of doped and codoped ZnO models shift up to conduction band, which reflects an n-type ZnO with good electrical conductivity can be obtained by Gd doping. In addition, the optical band gap is gradually increased with the incorporation of Al and Gd doping elements. Meanwhile, the optical band gap value of Gd^{+3}/Al^{+3}-codoped ZnO model was between those of Al-, Gd-doped ZnO models. Therefore, the visible absorption coefficients are slighly increased, compared to the pure and monodoped ZnO. These results are promising for experimental studies to explore other aspects, which remains inapplicable with codoping Gd/Al-codoped system.

Keywords: ZnO, Trivalent ions, Hybrid functional theory, Absorption, n-type conductivity.

References and Notes

1. G. Ghosh, A. Van de Walle, M. Asta, *Acta Mater*. **2008**, *56*, 3202.
2. F. Appel, J. D. H. Paul, M. Oehring, Gamma Titanium Aluminide Alloys: Science and Technology; Eds. Wiley: VCH: Weinheim, **2011**; Vol. 5, Chapter 6, pp 59-82.
3. F. Appel, H. Clemens, F.D. Fischer, *Prog. Mater. Sci.* **2016**, 81, 55–124.
4. H. Clemens, S. Mayer, *Adv. Eng. Mater.* **2013**, 15**,** 191.
5. B. T. Tan, J. Zhang, K. V. Sopiha, P. Wu, *Met. Mater. Int.* **2019**, 25, 869–879.
6. F. S. Sun, C. X. Cao, S. E. Kim, Y. T. Lee, M. G. Yan, *Metal. Mater. Trans. A.* **2011**, 32, 1573.
7. V. Kononikhina, A. Stark, W. Gan, A. Schreyer, F. Pyczak, *MRS. Adv.* **2017**, 2, 1399–1404.
8. F. Kong, N. Cui, Y. Chen, X. Wang, *Metal. Mater. Trans. A.* **2018**, 49, 5574–5584.
9. K. Hashimoto, *Mater. Sci. Forum*. **2012**, 706-709, 1066-1070.
10. K. Das, S. Das, *J. Mater. Sci.* **2003**, 38, 3995–4002.
11. S. L. Shu, C. Z. Tong, F. Qiu, Q. Zou, Q.-C. Jiang, *Can. Metall. Quart.* **2016,** 55, 156 – 160.
12. P. Erdely, P. Staron, A. Stark, T. Klein, H. Clemens, S. Mayer, *Acta Mater.* **2018**, 164, 110 – 121.
13. G. Liu, X. Li, Y. Su, D. Liu, J. Guo, H. Fu, *J. Alloys Comp.* **2012,** 541, 275–282.
14. G. Kresse, J. Furthmüller, *Comput. Mater. Sci.* **1996**, 6, 15.
15. G. Kresse, D. Joubert, *J. Phys. Rev. B.* **1999**, 59, 1758.

16. J.-P. Perdew, K. Burke, M. Ernzerhof, *Phys. Rev. Lett.* **1997**, 78, 1396.
17. N. Papanikolaou, R. Zeller, P.H. Dederichs, N. Stefanou, *Phys. Rev. B.* **1997**, 55, 4157.
18. J. Feng, B. Xiao, R. Zhou, W. Pan, D.R. Clarke, *J. Acta Mater.* **2012**, 60, 3380.
19. E.A. Brandes, Smithells Metal Reference Book; sixth Eds. Butterworth: London, 1983; Vol. 32, Chapter 2, pp 18-30.
20. B.J. Inkson, H. Clemens, J. Marien, *Scr. Mater.* **1998**, 38, 1377.
21. A. Hussaina, S. S. Hayatb, M. A. Choudhry, *Physica B* **2011,** 406, 1961–1965.
22. C. Jiang, *Acta. Mater.* 2008, 56, 6224–6231.
23. Y. Song, R. Yang, D. Li, Z. Q. Hub, Z. X. Guo, Intermetallics **2000**, 8, 563–568.
24. D. Holec, R. K. Reddy, T. Klein, H. Clemens, *J. Appl. Phys.* 2016, **119,** 205104.
25. X. P. Gao, Y. H. Jiang, R. Zhou, J. Feng, *J. Alloys Comp.* **2014,** 587, 819.
26. W. Voigt, Lehrbuch der Kristallphysik; Eds. Taubner: Leipzig, **1928**;
27. A. Reuss, Z. Angew, *Math. Mech.* **1929**, 9, 49.
28. R. Hill, *Proc. Phys. Soc. London, Sect. A.* **1952**, 65, 349.
29. X. Q. Chen, H. Niu, D. Li, Y. Li, Intermetallics **2011**, 19, 1275.
30. S.I. Ranganathan, M. Ostoja-Starzewski, *Phys. Rev. Lett.* **2008**, 101, 055504.
31. I. N. Frantsevich, F. F. Voronov, S. A. Bokuta, Elastic Constants and Elastic Moduli of Metals and Insulators, Eds. in: I.N. Frantsevich, NaukovaDumka, Kiev, **1983**; Vol. 12, Chapter 8, pp. 60.
32. M.E. Fine, L.D. Brown, H.L. Marcus, *Scr. Metall.* **1984**, 18**,** 951.
33. M. Alouani, R. C. Albers, M. Methfessel, Phys. Rev. B**. 1991,** 43, 6500.
34. X. Li-juan, X. Shu-long, C. Yu-yong, W. Juan, *Trans. Nonferrous Met. Soc. China* ***2012***, 22, 768−772.
35. M. Methfessel, A. T. Paxton, *Phys. Rev. B*, **1989**, 40, 3616–21.
36. Y. Jian, Z. Huang, J. Xing, L. Sun, Y. Liua, P. Gao, *Mater. Chem. Phys*. 2019, **221,** 311–321.
37. S. Mayer, P. Erdely, F. D. Fischer, D. Holec, M. Kastenhuber, T. Klein, H. Clemens, Adv. Eng. Mater. **2017,** 19, 1600735.
38. S. Mayer, C. Sailer, H. Nakashima, T. Schmoelzer, T. Lippmann, P. Staron, In:Symposium N-Intermetallic-Based Alloys for Structural and Functional Applications, MRS Proceedings 1295, **2011**.
39. K. Tanaka, K. Okamoto, H. Inui, Y. Minonishi, M.-Y. Amaguchi, M. Koiwa, *In: Philos. Mag. A.* **1996**, 73.5 1475.
40. J. H. Wang, Y. Lu, X.L. Zhang, X.-H. Shao, *Intermetallics* **2018,** 101, 1–7.
41. https://zaufre.quimica.uniovi.es/software.html#gibbs2.
42. A. Otero-de-la-Roza, V. Luana, Comput. Phys. Commun. **2011**, 182 1708.
43. F. Peng, H.Z. Fu, X.D. Yang, Physica B **2008,** 403 2851-2859.
44. A. V. Bakulin and S. E. Kulkova, J. Exp. Theor. Phys. **2018,** 127 1146–1158.

[1]

Division of Materials Discovery (DEPM), Unit of Research on Materials and Renewable Energies (URMER), University Abou Bekr Belkaid, B.P 119 Tlemcen 13000, Algeria.